Derivation of semiconductor laser mean-field and Swift-Hohenberg equations

J.-F. Mercier* and J. V. Moloney†
Department of Mathematics, University of Arizona, Tucson, Arizona 85721
(Received 22 May 2002; published 27 September 2002)

Bulk and quantum well semiconductor lasers by nature display fundamentally different physical characteristics relative to multilevel gas and solid state lasers. In particular, the refractive index is nonzero at peak gain and the peak gain can shift strongly with varying carrier density or temperature. Moreover, a quantum well laser gain may be strongly asymmetric if more than the lowest subband is populated. Rigorously computed and experimentally validated, gain and refractive index spectra are now available for a variety of quantum well structures emitting from the infrared to the visible. Active devices can be designed and grown such that the gain spectrum remains approximately parabolic for carrier density variations typically encountered in above threshold pumped broad area edge-emitting semiconductor lasers. Under this assumption, we derive a robust optical propagation model that tracks the important peak gain shifts and broadening as long as the gain remains approximately parabolic over the relevant energy range in a running laser. We next derive a multimode model where the longitudinal modes are projected out of the total field. The next stage is to derive a mean-field single longitudinal mode model for a wide aperture semiconductor laser. The mean-field model allows for significant cavity losses and widely different facet reflectivities such as occurs with antireflection- and high-reflectivity–coated facets. The single mode mean-field model is further reduced using an asymptotic expansion of the relevant physical fields with respect to a small parameter. The end result is a complex semiconductor Swift-Hohenberg description of a single longitudinal mode wide aperture laser. The latter should provide a useful model for studying scientifically and technologically important lasers such as vertical cavity surface emitting semiconductor lasers.

DOI: 10.1103/PhysRevE.66.036221 PACS number(s): 42.55.Px, 42.65.Sf

INTRODUCTION

Semiconductor lasers occupy a special niche in emerging optoelectronic technologies, offering compact size and very high bandwidth. The very large gain offered by these devices comes at a price however. In contrast to gas or other solid state lasers where simple few-level quantum mechanical descriptions suffice, semiconductor lasers involve complex many-body interactions within and between multicomponent plasmas [1,2]. Consequently, new features emerge which profoundly influence their operational characteristics. Of particular significance is a strong amplitude-phase coupling of the electric field and the shift of the semiconductor gain peak with varying carrier density or temperature. Significant gain line shape asymmetries typically occur when higher subbands in the quantum well (QW) become excited. A long standing problem with gain calculations is the inaccuracy of gain predictions in the neighborhood of the renormalized band edge. Gain formulations based on Lorentzian line shape functions tend to yield nonphysical absorption below the renormalized band edge. This nonphysical prediction was known to be due to an oversimplified treatment of polarization dephasing in the semiconductor material. The assumption that collisional dephasing could be treated at a rate equation level has been identified as the main culprit. The semiconductor line shape problem was only solved fairly recently when it was recognized that both diagonal and nondiagonal dephasing collisions needed to be treated at the full quantum kinetic level. A detailed review of this problem with relevant references to the earlier literature is contained in the textbook by Chow and Koch [3]. A surprising result of these calculations was that, not only did the nonphysical absorption below the band edge disappear, but so also did the strong falloff of the gain line shape near the band edge. In fact, the resultant gain line shape looks much more symmetric, in agreement with experimental gain measurements. A marked asymmetry in the gain only appears when higher confined subbands are populated.

A semiconductor laser theory which simultaneously incorporates full band structure, many-body dynamics, and propagation effects is beyond the existing or anticipated supercomputing capabilities. An alternative approach is to decouple the many-body physics from the the optical propagation and incorporate this as a quasiequilibrium optical response function that acts as a source term in Maxwell's equations. The approximation inherent in this approach is that the very fast (femtosecond) dynamics associated with many-body carrier-carrier and carrier-phonon scattering are slaved to the typically much slower (picosecond to nanosecond) dynamics of the semiconductor laser. One might argue that experimentally measured gain/absorption and refractive index spectra would provide the ideal input to an optical propagation model. However, reliable simultaneous experimental measurements of low-density absorption, high-density gain, and refractive index spectra are not widely available. Moreover, the various reduced model laser parameters derived in this paper would then appear as tabulated numbers rather than analytic expressions. The combination of rigorous band

*Permanent address: Laboratoire de Simulation et de Modélisation des Phénomènes de Propagation, ENSTA, URA 853 du CNRS, Paris, France; electronic address: jmercier@ensta.fr
†Electronic address: jml@dinha.acms.arizona.edu

structure and microscopic calculations only require as input the same band structure parameters that are available to the materials grower. No other adjustable parameters are needed. Convergent refractive index and linewidth enhancement factor spectra require the inclusion of detuned barrier states in addition to the well states. Experimental measurements of absorption, gain, and refractive index spectra across a broad range of active group III-V and II-VI single and multiple QW materials now match quantitatively with the full microscopic theory [4–7]. Databases for different active QW semiconductor materials can be built up beforehand and used directly as input to the optical propagation model.

Existing phenomenological theories of the semiconductor laser introduce a linewidth enhancement or α factor [8], which is a measure of the strength of the amplitude-phase coupling of the laser field. This quantity which is derived from the full microscopic theory as a linearization about the threshold carrier density, is a qualitative measure of the strong frequency chirp of pulses generated within semiconductor amplifiers or lasers and the strong transverse filamentation instabilities observed in high-power wide-aperture semiconductor lasers. Any derivation of a reduced order-parameter equation description of a semiconductor laser should reflect the presence of this quantity at leading order. Another unique aspect of the behavior of a semiconductor laser is the rather pronounced shift of the gain peak with varying carrier density and lattice temperature. This is particularly evident in wide-aperture single longitudinal mode lasers, such as vertical cavity surface emitting lasers (VCSELs) [9], where the relative location of the gain peak and cavity mode, strongly determines the transverse spatial intensity output.

Pattern formation in wide-aperture two-level lasers can be described by a systematic reduction of the full laser Maxwell-Bloch equations to a laser complex Swift-Hohenberg (CSH) equation [10,11]. An important conclusion from this work is that the latter amplitude equation description, although strictly valid in the neighborhood of the laser threshold, holds true even well beyond the onset of lasing. However, the single Swift-Hohenberg equation is not a good model to describe a class B laser. The model can be extended to include the mathematical stiffness of such laser systems by augmenting the CSH equation by a mean-flow describing the slow dynamics of the laser material inversion [10,11]. Later the model was extended in a phenomenological manner to apply to semiconductor lasers and to study the stabilization of the weak turbulence in semiconductor lasers using an optical feedback scheme [12]. The latter approach was capable of qualitatively capturing the filamentation instabilities experimentally observed in a wide-aperture semiconductor laser. Various other qualitative analytic approaches to treating the semiconductor gain and refractive index in optical propagation problems exist in the recent literature [13,14]. As stressed above, the details of semiconductor material growth strongly influences the latter physical properties so these phenomenological approaches add little insight into the behavior of real semiconductor lasers.

Our goal in this paper is to derive a self-consistent theoretical model of a semiconductor laser that incorporates the microscopically computed semiconductor response through simple fitting functions. This enables us to retain explicit analytic expressions throughout the theoretical development. As the running laser only accesses a finite fraction of the full multi-THz gain bandwidth and a finite range of carrier densities, we will restrict our current model to active semiconductor media with gain spectra that remain nearly parabolic in the relevant wavelength and carrier density range. We will also assume a fixed temperature in the laser. The latter restriction could be removed by adding a temperature equation and extending the gain tables in an extra physical dimension. We stress here that we are using the fully converged computed semiconductor line shape as input. As we can *a priori* determine whether the semiconductor active material fulfils the near-parabolic gain line shape requirement, we will use a simple Lorentzian fit to the line shape where the latter's parameters become functions of carrier density [15]. Any changes in the laser structure [i.e., QW width, depth, material composition, and nature of barrier regions (graded index self-confinement heterostructure versus self-confinement heterostructure, etc.)] will be reflected in changes in the laser equation coefficients. A secondary goal is to derive a physically self-consistent partial differential equation model from which single and multimode models can be derived. Here we want to allow for the fact that many low- and high-power edge emitters contain facets with high and low reflectivity coatings. Consequently the usual mean-field assumption will not work without some form of nonlinear coordinate transformation. The single longitudinal mode model will become the starting point for a further CSH reduction of the semiconductor laser equations valid for a wide-aperture single-longitudinal mode semiconductor laser. The latter provides a generalized rate equation description of such a laser. We will show that the linewidth enhancement factor α appears explicitly but that other contributions such as peak gain shift with density also make significant contributions.

The paper is organized as follows. The beginning of the paper will be concerned with the simplification of the effective Bloch equations (EBE) [15]. This model assumes that the physical gain can be approximated in the vicinity of its spectral peak by one or more Lorentzian functions. As mentioned above, this is a restriction on the applicability of the model presented here. In principle, this restriction could be lifted and the procedure outlined in this paper could be applied to the raw gain data. In Sec. I we generalize the EBE to the case of counterpropagating waves. Then we derive in Sec. II and Appendices A and B a set of coupled longitudinal mode equations valid for wide-aperture semiconductor lasers. Following this, we restrict the model to a single-longitudinal mode, retaining the transverse dependence, and obtain the mean-field effective Bloch equations (MFEBE). Section III concerns the derivation of the simplified MFEBE expressed with dimensionless variables: it starts with the linear stability analysis of the MFEBE in order to determine the lasing threshold. Then it becomes possible to define linear approximations versus the carrier density of the gain and of the refractive index.

In the end of the paper we derive the semiconductor CSH order-parameter equations. Section IV is devoted to the con-

struction of the neutral curves deduced from the linear stability analysis of the simplified MFEBE. Section V deals with the nonlinear analysis of the simplified MFEBE, leading both to the derivation of a SH equation and to the generalized rate equation model by including the mean flow [12].

I. STARTING MODEL: THE EFFECTIVE BLOCH EQUATIONS GENERALIZED TO COUNTERPROPAGATING WAVES

Starting from the full microscopic theory including many-body interactions, and using a Lorentzian approximation of the susceptibility $\chi(N,\omega)$, the Maxwell semiconductor Bloch equation model was derived [15]. This model resolves the full spatiotemporal (longitudinal and transverse) behavior of a general semiconductor amplifier or laser. Within this model, the susceptibility, which is critical to capturing the gain dispersion, is approximated by superposition of a background susceptibility frequency independent $\chi_0(N)$ and a Lorentzian

$$\chi(N,\omega)=\chi_0(N)+\frac{A(N)}{i\Gamma_0(N)+\delta_0+\omega-\delta(N)}, \qquad (1)$$

where $\delta_0=\omega_c-E_g/\hbar$ is the detuning parameter with E_g the bare band gap and ω_c the reference frequency, $A(N)$ determines the strength of the Lorentzian, $\Gamma_0(N)$ determines the bandwidth of the spectrum which changes with density, and $\delta_1(N)$ represents the gain peak shift with the density. In principle, multiple Lorentzians (poles) can be included in order to improve the fit to the gain and refractive index spectra over an arbitrary frequency bandwidth. For the present discussion, a single pole will suffice. An important point to note is that the gain spectra computed in the past using many-body theory for a variety of quantum well laser materials, show a pronounced asymmetry with a sharp rise in the gain near the band edge [1]. However, experimentally measured QW gain spectra do not display this feature—they look much more symmetric and bulklike. As mentioned in the Introduction, this discrepancy has now been resolved and recent many-body calculations show quantitative agreement with experiment [4–7]. The source of the discrepancy arose from ignoring nondiagonal scattering terms in the quantum Boltzmann description of the collisional relaxation terms appearing in the microscopic semiconductor Bloch equations [16]. This result means that the usual rate equation assumption made in this model is inappropriate and further justifies using a fitting procedure to the quantitatively computed gain spectra. Although gain spectral shapes could be accurately calculated with the improved approach, there still remained a strong discrepancy between experimentally measured linewidth enhancement or α factors and theory. This is not surprising as the latter involves a ratio of two differential quantities, the derivatives of the real and imaginary parts of the dielectric susceptibility, making this quantity very sensitive to small changes in the gain or refractive index. This open problem has just been solved by combining full band structure and many-body calculations which quantitatively include the nonresonant unconfined barrier states in addition to the confined well states [6]. With this result, we are now in a position to design a QW semiconductor amplifier and laser from the ground up, starting at the same point as the materials grower.

The electric and the polarization fields in a Fabry-Pérot cavity can be decomposed into a sum of forward and backward propagating fields,

$$E=E^+e^{i(Kz-\Omega_c t)}+E^-e^{i(-Kz-\Omega_c t)}+\text{c.c.},$$

$$\mathcal{P}=\mathcal{P}^+e^{i(Kz-\Omega_c t)}+\mathcal{P}^-e^{i(-Kz-\Omega_c t)}+\text{c.c.},$$

where $K=\Omega_c n_b/c$ is the optical wave vector in the medium of background index n_b, with c being the speed of light in the vacuum, and the z axis is perpendicular to the two mirrors of the Fabry-Pérot cavity. The index $+$ designates the forward field, the index $-$ designates the backward field, and c.c. refers to the complex conjugated quantity.

The effective Bloch equations generalized to the case of counterpropagating waves are [17]

$$\frac{\partial E^\pm}{\partial t}\pm\frac{c}{n_g}\frac{\partial E^\pm}{\partial z}=\frac{ic}{2n_g}\left\{\frac{1}{K}\nabla^2E^\pm+K\Gamma\left[\chi_0(N)E^\pm+\frac{P^\pm}{\epsilon_0\epsilon_b}\right]\right\},$$

$$\frac{\partial P^\pm}{\partial t}=\{-\Gamma_0(N)+i[\delta_0-\delta(N)]\}P^\pm-i\epsilon_0\epsilon_bA(N)E^\pm,$$

$$\frac{\partial N}{\partial t}=D_N\nabla^2N-\gamma_nN+\frac{\eta J}{ew}+\frac{i}{4\hbar}\{\epsilon_0\epsilon_b[\chi_0^*(N)-\chi_0(N)]\times(|E^+|^2+|E^-|^2)+P^+{}^*E^+-P^+E^+{}^*+P^-{}^*E^--P^-E^-{}^*\},$$

where n_g is the group index, Γ the confinement factor, the operator ∇^2 represents

$$\nabla^2=\frac{\partial^2}{\partial x^2}+\frac{\partial^2}{\partial y^2},$$

and D_N is the diffusion constant of the carrier diffusion term in the lateral directions x and y. The parameter η, J, e, and w are, respectively, the quantum efficiency, pumping current, electron charge, and active region thickness. * designs the complex conjugated quantity. When describing edge emitting lasers the transverse Laplacian operator is replaced by $\partial^2/\partial x^2$.

II. MEAN-FIELD APPROXIMATION

The derivation of the mean-field model from the full counterpropagating effective Bloch equations is presented in Appendices A and B. Here we summarize the key results. The derivation consists first in introducing a transformation of the counterpropagating optical field envelops in order to obtain new field amplitudes obeying standard ideal mirror boundary conditions (Appendix A). By unfolding the cavity it becomes possible to introduce a Fourier longitudinal mode decomposition. The previous transformation needs the introduction of a mean reflectivity R defined as the square root of the product of the two reflectivities R_1 and R_2 of both mirrors. Extending the procedure for a ring cavity [18], we obtain a coupled mode decomposition (Appendix B).

The mean-field, single-longitudinal mode, model equations read

$$\frac{\partial E}{\partial t} = -\frac{c|\ln R|}{2n_g L}E + \frac{ic}{2n_g}\left\{\frac{1}{K}\nabla^2 E + K\Gamma\left[\chi_0(N)E + \frac{P}{\epsilon_0\epsilon_b}\right]\right\}, \tag{2}$$

$$\frac{\partial P}{\partial t} = \{-\Gamma_0(N) + i[\delta_0 - \delta(N)]\}P - i\epsilon_0\epsilon_b A(N)E, \tag{3}$$

$$\frac{\partial N}{\partial t} = D_N\nabla^2 N - \gamma_n(N-N_0) + \frac{i}{4\hbar}\frac{1-R^2}{R|\ln R|}\{\epsilon_0\epsilon_b[\chi_0(N)^* - \chi_0(N)]|E|^2 + P^*E - PE^*\}.$$

This system of equations will form the basis for the derivation of the semiconductor laser complex Swift-Hohenberg equation in the following sections. The physics of the laser gain material is contained in the single pole model fits and these capture density dependent gain bandwidth variation, peak gain shift, low-density absorption, and variation of an effective α-factor spectrum. We note here also that this system of equations allows us to consider realistic semiconductor laser devices that have very different facet reflectivities as would be the case with lasers having AR- and HR-coated facets. The usual mean-field limit corresponds to the mean reflectivity $R \to 1$ as would be the case for low-power VCSELs. High-power wide-aperture vertical external cavity semiconductor lasers (VECSELs), on the other hand, contain multiple quantum well stacks to increase the single pass gain and they typically can accommodate facet losses significantly less than unity. The geometric cavity factor (dependent on R) will then be expected to modify the stimulated emission term on the right-hand side of the carrier density equation.

The electric field and carrier density evolution equations are close to the system obtained in the case of a lossy semiconductor laser [19]. The mean-field model in Ref. [19] has been compared to a full counterpropagating wave code and showed good agreement.

As we will be interested in the derivation of an amplitude description valid near threshold, we will use linear approximations to the background susceptibility $\chi_0(N)$, the strength of the Lorentzian $A(N)$, the bandwidth of the spectrum $\Gamma_0(N)$, and the gain peak shift with the density $\delta(N)$. These quantities will be expanded around a threshold value N_c of the injected carrier density N_0. These assumptions are justified by the observation that the carrier density remains approximately clamped near its threshold value above lasing threshold. Note that the carrier density itself may be strongly nonuniform along the device but what we are referring to here is the z-averaged density. We need first to determine the threshold carrier density N_c around which to expand the above functions.

III. APPROXIMATION OF THE MEAN-FIELD EFFECTIVE BLOCH EQUATIONS

A. Linear stability analysis

Below threshold, the solution of the MFEBE is the nonlasing solution $E=0=P$ and $N=N_0$. When the injected carrier density N_0 reaches the threshold carrier density N_c, the nonlasing solution is unstable and an instability of wave vector $\vec{q}$ and of frequency ω can develop. This instability is sought in the form

$$E = \overline{E}\ e^{i(q_x\vec{x} + q_y\vec{y} - \omega t)},$$

$$P = \overline{P}\ e^{i(q_x\vec{x} + q_y\vec{y} - \omega t)},$$

$$N = N_0 + \overline{N},$$

where $\overline{E}$, $\overline{P}$, and $\overline{N}$ are constants. Eliminating $\overline{P}$ from Eqs. (2) and (3) we deduce that the electric field satisfies

$$-i\omega\overline{E} = -\kappa\overline{E} + \frac{ic}{2n_g}\left[\frac{1}{K}(-q^2)\overline{E} + K\Gamma\chi(N_0,\omega)\overline{E}\right], \tag{4}$$

where $\kappa = c|\ln R|/2n_g L$ [Eq. (A4) of Appendix A]. We introduce the modal gain G defined by

$$G(N_0,\omega) = -\frac{cK\Gamma}{2n_g}\chi''(N_0,\omega) = \frac{cK\Gamma}{2n_g}\left\{\frac{A(N_0)\Gamma_0(N_0)}{\Gamma_0(N_0)^2 + [\omega + \delta_0 - \delta(N_0)]^2} - \chi_0''(N_0)\right\},$$

using the Lorentzian approximation for the susceptibility [Eq. (1)]. We also define the function

$$f(N_0,\omega) = \omega + \frac{cK\Gamma}{2n_g}\left\{\chi_0'(N_0) + \frac{A(N_0)[\omega + \delta_0 - \delta(N_0)]}{\Gamma_0(N_0)^2 + [\omega + \delta_0 - \delta(N_0)]^2}\right\}.$$

Then introducing the real part χ' and the imaginary part χ'' of the susceptibility, the real part and imaginary part of Eq. (4) read, respectively,

$$G(N_0,\omega) = \kappa, \tag{5}$$

$$\frac{c}{2n_g K}\ q^2 = f(N_0,\omega). \tag{6}$$

Equation (5) defines the threshold at which the laser turns on: the threshold is reached when the amplification of the electric field measured by the gain balances the attenuation of the electric field due to the losses κ. This is achieved when the pump density reaches the value $N_0 = N_{0c}$. The sec-

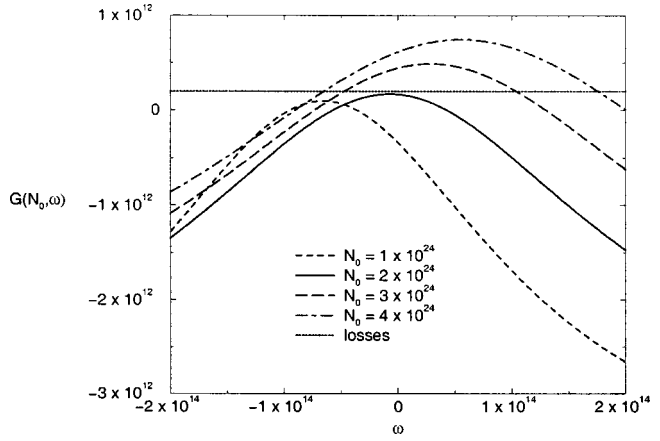

FIG. 1. Variations of the Lorentzian approximation of the gain ($\mathrm{rad\,s^{-1}}$) vs the frequency ω ($\mathrm{rad\,s^{-1}}$) for several values of the injected carrier density N_0 ($\mathrm{m^{-3}}$) ($L=200$ μm, $R=30\%$, $n_b=3.6$, $n_g=4.6$, $\Gamma=0.25$, $\Omega_c=1.42$ eV, $\eta=0.95$, $\gamma_n=2\times10^{-9}$ $\mathrm{s^{-1}}$, $D_N=18\times10^{-12}$ $\mathrm{m^2\,s^{-1}}$, $w=10^{-8}$ m).

ond equation is the generalization of the frequency pulling condition extended to a wide-aperture laser.

Once the fitting functions are tabulated for a particular QW gain medium, the lasing threshold can be determined. The threshold pump carrier density N_{0c} is determined from the simultaneous solution of these two equations. The threshold for a plane wave or transverse spatially homogeneous mode laser is obtained by setting $|q|=0$. For a GaAs laser the coefficients $\chi_0(N)$, $A(N)$, $\Gamma_0(N)$, and $\delta(N)$ involved in the Lorentzian approximation of the susceptibility have been calculated as rational functions versus the carrier density N [19]. Using these expressions we can calculate explicitly the gain. In a characteristic Fabry-Pérot cavity of length $L=200$ μm and of mean reflectivity $R=30\%$, the evolution of the gain $G(N_0,\omega)$ when the frequency ω varies is represented in Fig. 1 for values of the injected carrier density N_0 varying in the range $[1\times10^{24}\ \mathrm{m^{-3}},4\times10^{24}\ \mathrm{m^{-3}}]$. The losses $\kappa=1.963\times10^{12}\ \mathrm{rad\,s^{-1}}$ are represented as a horizontal line. The frequency ω is a detuning relative to an absolute frequency (or energy of 1.42 eV). The latter is chosen to match the peak of the Lorentzian fit to the absolute frequency location of the peak gain of bulk GaAs at the threshold density. Finite values of ω correspond to frequency pulling relative to this absolute value.

When N_0 is fixed, $G(N_0,\omega)$ presents a maximum located in the frequency $\omega_{max}(N_0)=\delta(N_0)-\delta_0$. The associated maximum value of $G(N_0,\omega)$ is

$$G_{max}(N_0)=\frac{cK\Gamma}{2n_g}\left[\frac{A(N_0)}{\Gamma_0(N_0)}-\chi_0''(N_0)\right]. \tag{7}$$

The threshold is reached when the equality, Eq. (5), is satisfied and thus at least when $G_{max}(N_0)\geqslant\kappa$. We see in Fig. 1 that for both the injected carrier density values $N_0=1\times10^{24}\ \mathrm{m^{-3}}$ and $N_0=2\times10^{24}\ \mathrm{m^{-3}}$ the gain is always lower than the losses and no frequency can satisfy Eq. (5). On the contrary, for the injected carrier density values N_0 equal to or larger than $3\times10^{24}\ \mathrm{m^{-3}}$ a range of frequencies for which the gain is larger than the losses exists. In the case $R=30\%$, the threshold carrier density is $N_c=2.09\times10^{24}\ \mathrm{m^{-3}}$ and the corresponding perturbation wave number, deduced from Eq. (6), is equal to $q_c=1.202$ $\mu\mathrm{m^{-1}}$.

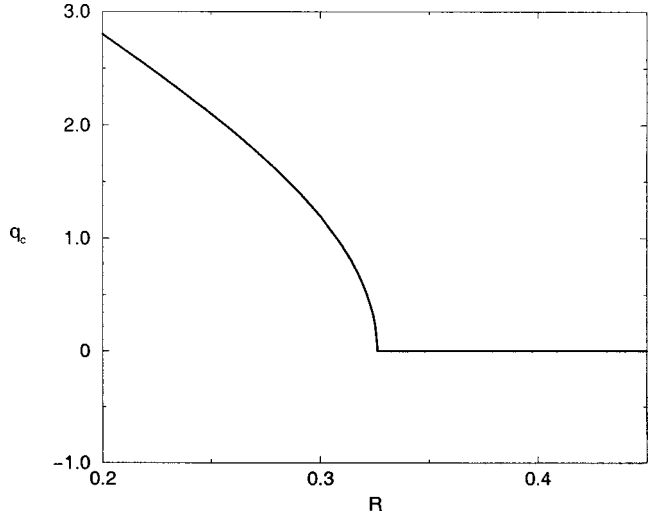

FIG. 2. Critical wave number q_c (in $\mu\mathrm{m^{-1}}$) vs the mean reflectivity R.

We have solved Eqs. (5) and (6) for various values of R for the same laser of length $L=200$ μm as considered in Fig. 1. The critical value q_c of the wave number is represented in Fig. 2 versus R. Corresponding values of N_c and of ω_c versus R are drawn on Figs. 3 and 4. We see in Fig. 2 that there exists a sharp transition from finite off axis to plane wave emission at lasing threshold as the mean reflectivity R exceeds a finite value. The transition from $q_c\neq0$ to $q_c=0$ occurs for the mirror reflectivity value $R=0.326$. Inspection of Fig. 3 shows that the carrier density decreases with increasing reflectivity R. At the value $R=0.326$, the normalized critical density $N_c=2.09$. This is the point at which peak gain in Fig. 2 moves from positive to negative detuning. Therefore for reflectivities below $R=0.326$, the laser emits

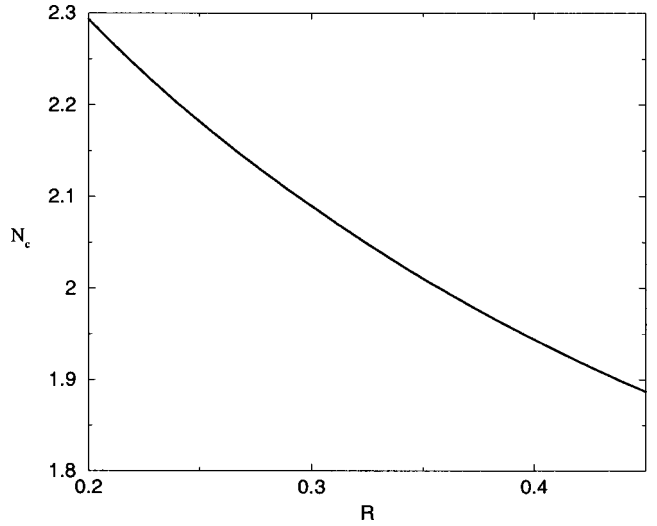

FIG. 3. Critical injected carrier density N_c ($\times10^{24}\ \mathrm{m^{-3}}$) vs the mean reflectivity R.

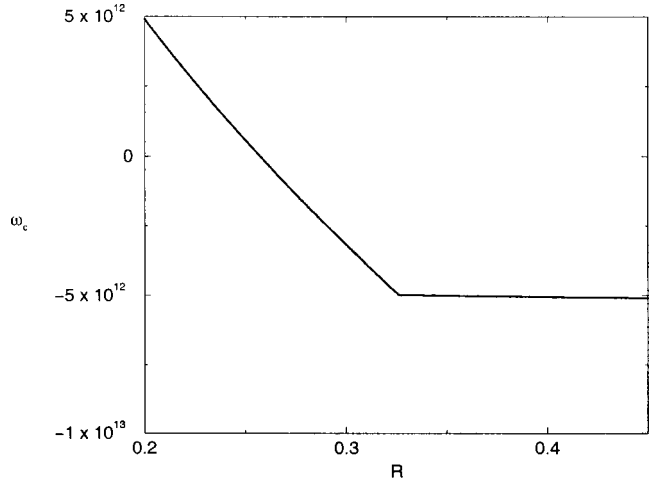

FIG. 4. Critical frequency ω_c (rad s^{-1}) vs the mean reflectivity R.

in an off-axis mode at threshold while for higher reflectivities, it emits in a quasi-plane-wave (fundamental) mode [20].

1. Case of a positive critical wave number

For small values of the mean mirror reflectivity $R<0.326$, the threshold carrier density N_c is found to satisfy

$$G_{max}(N_c)=\kappa. \tag{8}$$

Therefore we have an exact balance between the maximum of the injected energy in the laser cavity and the losses on the mirrors. The critical frequency is

$$\omega_c=\omega_{max}(N_c)=\delta(N_c)-\delta_0, \tag{9}$$

while q_c is deduced from Eq. (6).

2. Case of a zero critical wave number

For $R>0.326$, we obtain $q_c=0$, while Eqs. (8) and (9) no longer apply. The relation between N_c and ω_c is more complicated than previously and will be detailed later with nondimensional variables (Sec. III C). This is obvious when looking at Fig. 4: the curve presents a slope break in $R=0.326$, and the critical frequency remains nearly constant for $R>0.326$. For the particular case $R=0.45$ we find $N_c=1.89\ 10^{24}\ \mathrm{m}^{-3}$ and $\omega_c=-0.509\times10^{13}\ \mathrm{rad\,s}^{-1}$.

B. Simplified mean-field effective Bloch equations

Having determined the threshold carrier density we are able to introduce linear approximations of the Lorentzian coefficients, defined around the value of the injected carrier density N_c. Noting with a single index the values of the coefficients defining the Lorentzian approximation of the susceptibility evaluated at $N=N_c$ we can write

$$A(N)=A_1+A_2(N-N_c),$$

$$\chi_0(N)=\chi_1+\chi_2(N-N_c),$$

$$\Gamma_0(N)=\Gamma_1+\Gamma_2(N-N_c),$$

$$\delta(N)=\delta_1+\delta_2(N-N_c).$$

Note that the coefficients A_i, χ_i, Γ_i, and δ_i for $i=1,2$ are not exactly the ones defined in Appendix B. We have chosen not to complicate notation. These expansions are valid only close to threshold, when N_0 and N are close to N_c. We introduce the new carrier density $N'=N-N_0$, and the corrected imaginary part of the background susceptibility $\rho_1=\chi_1''+2n_g\kappa/cK\Gamma$. The MFEBE take the form

$$\frac{\partial E}{\partial t}=\frac{ic}{2n_g}\left\{\frac{1}{K}\nabla^2E+K\Gamma\left[\frac{P}{\epsilon_0\epsilon_b}+[\chi_1'+i\rho_1+\chi_2(N_0-N_c)]E+\chi_2N'E\right]\right\},$$

$$\frac{\partial P}{\partial t}=-[\Gamma_1+i(\delta_1-\delta_0)+(\Gamma_2+i\delta_2)(N_0-N_c)+(\Gamma_2+i\delta_2)N']P-i\epsilon_0\epsilon_b\{[A_1+A_2(N_0-N_c)]E+N'E\},$$

$$\frac{\partial N'}{\partial t}=D_N\nabla^2N'-\gamma_nN'+\frac{i}{4\hbar}\frac{1-R^2}{R|\ln R|}\{-2i\epsilon_0\epsilon_b[\chi_1''+\chi_2''(N_0-N_c)+\chi_2''N']|E|^2+P^*E-PE^*\}.$$

ρ_1 represents the total loss of energy in the cavity: the loss due to the interaction between the light and the medium proportional to the imaginary part of the susceptibility $\chi_1''=\chi''(N_c)$ and the loss through the mirrors of the Fabry-Pérot cavity proportional to the logarithm of the mean reflectivity R. The variable change $N'=N-N_0$ is chosen instead of the change $N'=N-N_c$, because it introduces the difference N_0-N_c which will be used as a control parameter.

These equations have a form close to the Maxwell-Bloch equations which describe a two-level laser [21]. Starting from the Maxwell-Bloch equation for two-level lasers written in complex Lorentz notation [22], these equations were proved to be interesting for laser modeling since they can be reduced to order parameter descriptions in the form of Swift-Hohenberg equations [10,11]. The MFEBE may also be written in complex Lorenz notation with a form close to the Maxwell-Bloch equations, by making the following change of variables:

$$t' = \Gamma_1 t,$$

$$E = i\Gamma_1 \sqrt{\frac{2\hbar R|\ln R|}{\epsilon_0 \epsilon_b A_2 (1-R^2)}}\; e^{i\sigma dt} e,$$

$$P = \Gamma_1 \rho_1 \sqrt{\frac{2\hbar R|\ln R|\epsilon_0 \epsilon_b}{A_2(1-R^2)}}\; e^{i\sigma dt} p,$$

$$N = -\frac{\rho_1 \Gamma_1}{A_2} n,$$

where $\sigma = cK\Gamma\rho_1/2n_g\Gamma_1$ and $d = \chi_1'/\rho_1$. The MFEBE then read, suppressing the prime of the new time t',

$$\frac{\partial e}{\partial t} = ia\nabla^2 e + \sigma[p - e + i(j+ik)(r - r_c - n)e],$$

$$\frac{\partial p}{\partial t} = -[1 + i\eta + (u+iv)(r - r_c - n)]p + (r-n)e, \tag{10}$$

$$\frac{\partial n}{\partial t} = -bn + c\nabla^2 n + \frac{1}{2}(e^* p + e p^*) - [f + k(r - r_c - n)]|e|^2,$$

where the coefficients are defined as

$$a = \frac{c}{2n_g K \Gamma_1}, \qquad u + iv = \frac{(\Gamma_2 + i\delta_2)\rho_1}{A_2},$$

$$\Omega = \frac{\delta_1 - \delta_0}{\Gamma_1}, \qquad r = \frac{A_1 + A_2(N_0 - N_c)}{\rho_1 \Gamma_1},$$

$$d + if = \frac{\chi_1}{\rho_1}, \qquad b = \frac{\gamma_n}{\Gamma_1},$$

$$j + ik = \frac{\chi_2 \Gamma_1}{A_2}, \qquad c = \frac{D_N}{\Gamma_1}.$$

We have also introduced the new detuning $\eta = \Omega + \sigma d$ and the threshold value r_c of the pumping parameter, defined as r evaluated at $N_0 = N_c$,

$$r_c = \frac{A_1}{\rho_1 \Gamma_1}. \tag{11}$$

This system is called the simplified mean-field effective Bloch equations (SMFEBE), since the fitting functions involved in the microscopic semiconductor response have been reduced to linear expansions.

If we compare this linearized system to the Maxwell-Bloch equations, we see the following differences: first of all some new complex terms appear, essentially linked to the Lorentzian approximation of the susceptibility. $(d+if)$ and $(j+ik)$ represent, respectively, the constant part χ_1 and the derivative with respect to the carrier density χ_2 of the background susceptibility χ_0, written in a nondimensional form. u and v represent the derivatives with respect to the carrier density, respectively, of the bandwidth of the spectrum (term Γ_2) and of the gain peak shift with the density (term δ_2). The last new term is the diffusion of the carrier density $c\nabla^2 n$ appearing in the equation for the evolution of the carrier density. It is interesting to notice that the Maxwell-Bloch equations can be exactly recovered from this set of equations by setting the new parameters c, d, f, j, k, u, and v, to zero. As in the Maxwell-Bloch model, the pumping parameter r is still proportional to the injected current and therefore to N_0, but also depends on the strength of the Lorentzian. Comparing this system to the Maxwell-Bloch equations, we see that the temporal evolution of the electric and polarization field and the carrier density depends on the pumping parameter for a semiconductor laser, whereas only the temporal evolution of the polarization field is depending on the pumping parameter in the Maxwell-Bloch model. This property will complicate the determination of the lasing threshold of the simplified MFEBE: whereas the threshold was obtained explicity as a function of the perturbation wave number in the case of the Maxwell-Bloch model [10,11], the threshold will be found as a root of a polynomial.

C. Values of the dimensionless critical parameters r_c and q_c

When studying the lasing threshold we encountered two situations according to the value of the losses in the laser measured by R: $q_c \neq 0$ or $q_c = 0$. In both situations we will now express r_c and q_c in terms of the coefficients appearing in the SMFEBE.

1. Case $q_c \neq 0$

In this first situation the threshold corresponds to an exact balance between the maximum of the gain and the losses. The maximum of the gain is located at the critical frequency $\omega_c = \delta_1 - \delta_0$ [Eq. (9)], and attains the value [Eqs. (7) and (8)]

$$\kappa = \frac{cK\Gamma}{2n_g}\left(\frac{A_1}{\Gamma_1} - \chi_1''\right).$$

Therefore using Eq. (11) and the relation $\rho_1 = \chi_1'' + 2n_g\kappa/cK\Gamma$ we find that the critical pumping parameter is $r_c = 1$. The critical perturbation wave number q_c is defined, using Eq. (6), by the relation

$$\frac{c}{2n_g K}\; q_c^2 = f(N_c, \omega_c) = \delta_1 - \delta_0 + \frac{c\kappa\Gamma\chi_1'}{2n_g}.$$

Dividing by Γ_1 and defining the new effective detuning

$$\eta = \frac{\delta_1 - \delta_0}{\Gamma_1} + \frac{c\kappa\Gamma\chi_1'}{2n_g\Gamma_1}, \tag{12}$$

we are led to the relation $aq_c^2 = \eta$. This parabolic law is consistent with the behavior of q_c versus R for $R < 0.326$ (Fig. 2).

2. Case $q_c=0$

These results are valid as long as the detuning η is positive, since $q_c^2=\eta/a$. If $\eta\leqslant 0$ we are in the case of a plane wave laser $q_c=0$. Introducing the dimensionless frequency $x=(\omega_c+\delta_0-\delta_1)/\Gamma_1$, the energy balance Eq. (5), and the dispersion relation Eq. (6) evaluated at $q=0$ and divided by Γ_1 read

$$\frac{A_1}{\Gamma_1}\frac{1}{1+x^2}=\rho_1, \tag{13}$$

$$0=x+\frac{\delta_1-\delta_0}{\Gamma_1}+\frac{c\kappa\Gamma}{2n_g\Gamma_1}\left(\frac{A_1}{\Gamma_1}\frac{x}{1+x^2}+\chi_1'\right). \tag{14}$$

The critical pumping parameter [Eq. (11)] can be expressed as a function of the dimensionless frequency thanks to Eq. (13): $r_c=1+x^2$. Last using the value of the detuning [Eq. (12)], the value of the parameter σ and Eq. (13), Eq. (14) simply becomes $0=x(1+\sigma)+\eta$. Thus $r_c=1+(\eta/1+\sigma)^2$.

In the case of a two-level laser described by the Maxwell-Bloch equations [10,11], the same results were found except that the square of the perturbation wave number was linked to the detuning Ω instead of the new detuning η. It was concluded that Ω was a control parameter leading to different type of bifurcation of the nonlasing solution above threshold according to the sign of Ω. For a semiconductor laser, η is the effective control parameter. For positive values of the detuning, the critical pumping parameter is $r_c=1$ and the critical perturbation wave number is $q_c=\pm\sqrt{\eta/a}$, whereas for negative values of η, $r_c=1+(\eta/1+\sigma)^2$ and $q_c=0$. In the following paragraph we will be interested in the behavior of the laser when the wave number is slightly above its critical value and thus we will determine the neutral curves, i.e., the variations of the pumping parameter $r(q)$ versus q.

IV. NEUTRAL CURVES

We look for a perturbation of the nonlasing solution $e=0=p=n$ of Eq. (10) in the form $(e,p)=(\overline{e},\overline{p})\ e^{i(q_x x+q_y y)+\lambda t}$ and $n=\overline{n}$, where $\vec{q}=q_x\vec{x}+q_y\vec{y}$ is the perturbation wave vector and λ is the complex temporal growth rate. The amplitudes $\overline{e}$, $\overline{p}$, and $\overline{n}$ are considered small in order to be able to linearize Eq. (10). We decompose the growth rate in the form $\lambda=s+i\omega$ where s is the real temporal growth rate and ω the frequency of the perturbations. Using Eq. (10), the amplitudes $\overline{e}$ and $\overline{p}$ are found to be solution of the system

$$\begin{aligned}&[s+\sigma+i(\omega+aq^2)-i\sigma(j+i\ \ k)(r-r_c)]\overline{e}=\sigma\overline{p},\\ &\{[s+1+i(\omega+\eta)+(u+iv)(r-r_c)]\overline{p}\}=r\overline{e},\end{aligned} \tag{15}$$

where $q=\sqrt{q_x^2+q_y^2}$ is the modulus of the perturbation wave number in the general case or $q=q_x$ in the one-dimensional case.

A. Dispersion relation

The determinant of the system Eq. (15) must vanish to get a nontrivial solution. Introducing the following functions depending on the detuning η (through the critical pumping parameter r_c), and on the pumping parameter r:

$$\begin{aligned}J(\eta,r)&=\sigma j(r-r_c),\\ K(\eta,r)&=\sigma[1+k(r-r_c)],\\ U(\eta,r)&=1+u(r-r_c),\\ V(\eta,r)&=v(r-r_c),\end{aligned} \tag{16}$$

the cancelation of the determinant leads to the dispersion relation

$$[s+K+i(\omega+aq^2-J)][s+U+i(\omega+\eta+V)]=\sigma r. \tag{17}$$

Taking the real and imaginary parts of Eq. (17) and eliminating the frequency leads to a transcendental equation that the threshold value of the pumping parameter r must satisfy

$$\sigma r=(s+K)(s+U)\left[1+\left(\frac{\eta-aq^2+J+V}{2s+K+U}\right)^2\right]. \tag{18}$$

At threshold, the real part s of the temporal growth rate λ vanishes and the pumping parameter becomes a solution of

$$\sigma r=KU\left[1+\left(\frac{\eta-aq^2+J+V}{K+U}\right)^2\right], \tag{19}$$

whereas the frequency is linked to the pumping parameter by the relation

$$\omega=U\left(\frac{\eta-aq^2+J+V}{K+U}\right)-\eta-V. \tag{20}$$

Equation (19) may be written as an order four polynomial in the r variable. Therefore a numerical procedure is necessary in order to draw the neutral curves. However, results concerning the threshold can of course be easily recovered: the threshold corresponds to $r=r_c$ and $q=q_c$, and introducing these values in Eq. (19) leads to the critical value of the pumping parameter $r_c=1+(\eta-aq_c^2/1+\sigma)^2$, and Eq. (20) yields the critical value of the frequency $\omega_c=-(\sigma\eta+aq_c^2/1+\sigma)$, where the critical perturbation wave number q_c satisfies $q_c=0$ if $\eta<0$ and $q_c^2=\eta/a$ if $\eta>0$. Above threshold ($r>r_c$), linearization of Eq. (10) is no longer possible because the perturbations e, p, and n become large, and nonlinear terms must be taken into account. Using an amplitude equation method, simpler nonlinear equations can be deduced. To achieve this goal the typical temporal and spatial scales of the variables involved in the amplitude equation need first to be determined. This can be achieved by studying the local behavior of the pumping parameter versus the detuning η and versus the wave number q when this latter parameter varies around its critical value q_c.

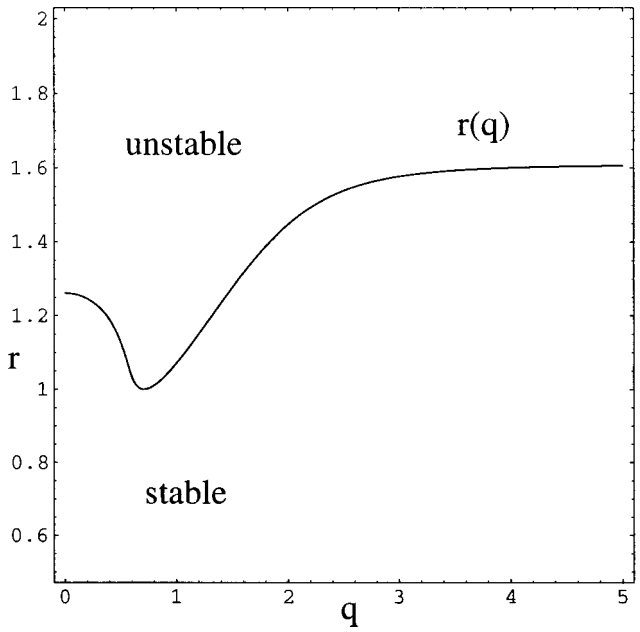

FIG. 5. Neutral curve $r(q)$ for a detuning $\eta=0.5$.

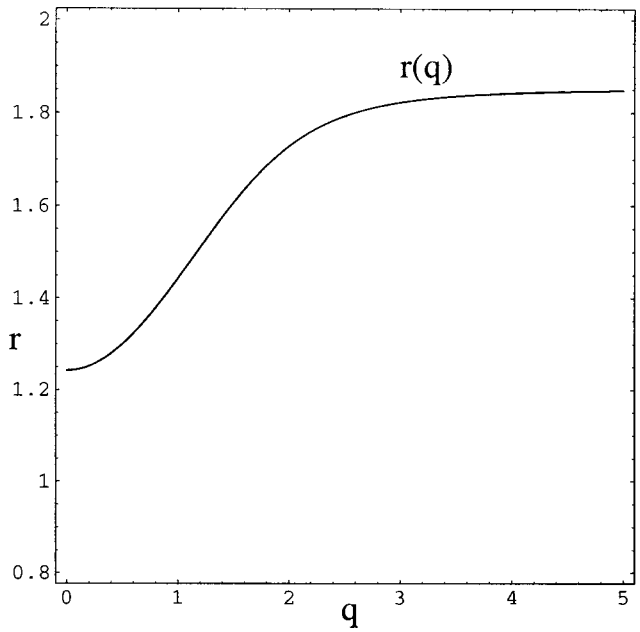

FIG. 6. Neutral curve for a negative detuning $\eta=-0.5$.

In the case of a two-level laser, since the dispersion relation was found analytically, the deviation form threshold $r-r_c$ was obtained to vary explicitely like $(q-q_c)^2$ close to threshold when the detuning is different from zero, and to vary like $(q-q_c)^4$ when $\Omega=0$ [10,11]. Thus it was concluded that the slow space variables must depend on $(r-r_c)^{1/4}$ when the detuning is taken close to zero. In our case, the link between r and q is not explicit, and we need to draw the neutral curves in order to find the power n such that $r-r_c$ varies like $(q-q_c)^n$ around threshold. Therefore in the following paragraph we will determine the changes in the shape of the neutral curves $r(q)$ solution of Eq. (19) versus the perturbation wave number when the detuning varies.

B. Construction of the neutral curves

Equation 19 is invariant under the transformation $q\rightarrow -q$ so the solutions $r(q)$ are even functions, and we will just give the behavior of the neutral curves for positive values of the perturbation wave number.

1. Case of a positive detuning

In the case of a positive detuning, the critical pumping parameter takes the value $r_c=1$. Introducing this value in the definition of the four intermediate functions defined in Eq. (16) and solving the dispersion relation Eq. (19), the neutral curves $r(q)$ can be calculated. The value of the coefficient a of the diffraction term in Eq. (10) can be taken equal to 1: indeed the spatial coordinates x and y in Eq. (10) are dimensional variables. Introducing the nondimensional spatial coordinates $\tilde{x}$ and $\tilde{y}$ defined by $x=l\tilde{x}$ and $y=l\tilde{y}$ where l is a reference length, the evolution equation of the electric field in the system Eq. (10) can be rewritten in a nondimensional form. The new diffraction coefficient $\tilde{a}=a/l^2$ is equal to 1 if we choose a reference length equal to $l=\sqrt{a}$. The other values of the parameters in the simplified MFEBE are deduced from Ref. [15]. In the case of a 200 μm long laser corresponding to a threshold carrier density $N_c=2.09\times10^{24}$ m^{-3}, these values are $\sigma=0.016$, $j=-0.0041$, $k=-1.64$, $u=1.54$, and $v=2.18$.

Figure 5 shows the neutral curve in the case of the value of the detuning $\eta=0.5$. It appears that for each value of the wave number, Eq. (19) admits two real roots, and two complex roots. The two complex roots and one real root do not correspond to physical behavior. The real root with the smallest magnitude is independent of the perturbation wave number q and is a nonphysical artifact of the linear approximation of the coefficients appearing in the Lorentzian approximation to the susceptibility. We will only discuss the behavior of the real physical root. This root $r(q)$ has a minimum located at $q=0.71$ with value $r=1$.

We have also studied the variations of the sign of the real temporal growth rate s when r and q are varying, solving Eq. (18). The usual situation in linear stability analysis is recovered: for a fixed value of the perturbation wave number, when the value of the pumping parameter r is below the critical value $r(q)$, the laser is stable and when r exceeds $r(q)$ the perturbation of the nonlasing solution becomes unstable. Domains of stability and unstability are indicated on Fig. 5.

2. Case of a negative detuning

In the case $\eta<0$ the critical value of the pumping parameter is equal to $r_c=1+(\eta/1+\sigma)^2$. When the detuning is taken equal to $\eta=-0.5$ and thus $r_c=1.24$, the neutral curves take the form represented in Fig. 6. The minimum of the root $r(q)$ is now located at the wave number $q_c=0$ and corresponds to the critical pumping parameter $r(0)=r_c=1.24$.

V. WEAKLY NONLINEAR ANALYSIS

We will now derive a Swift-Hohenberg equation from the simplified MFEBE. The preceding paragraph has confirmed

that the nature of the bifurcation changes depending on the sign of the detuning. In order to capture the behavior of the simplified MFEBE equations for both signs of η, we assumed the detuning small and a small parameter ϵ is introduced. Then we define $\eta=\epsilon\ \eta_1$ and look for solutions (e,p,n) in the form of a power series expansion in the small parameter ϵ. The laser variables also depend on slow temporal and spatial scales that we will determine in the following paragraphs. As in the case of a two-level laser, analytical results are necessary to derive an amplitude equation: this is achieved by developing the dispersion relation as an expansion in the small quantity $q-q_c$.

A. Determination of the slow time and space variables

For $\eta=0$, the threshold is located at the wave number $q_c=0$, in the critical pumping parameter $r_c=1$, and is associated with the frequency $\omega_c=0$. To calculate the slow space scales we need to determine how the pumping parameter r is varying versus the perturbation wave number about its critical value $r_c=1$. Keeping the detuning equal to $\eta=0$, if we let the perturbation wave number vary a little from its critical value, namely, q small, then the pumping parameter may be written as $r=1+\rho$ where the introduced parameter ρ is also small. From the dispersion relation Eq. (19) we obtain at the lowest order in the deviation from threshold ρ and in the small wave number q a link between ρ and q,

$$(1-k-u)\rho+O(\rho^2)=\left[\frac{-aq^2+(\sigma j+v)\rho}{\sigma+1}\right]^2[1+O(\rho)], \tag{21}$$

where $O(\rho)$ designs a function of order ρ. Looking for the parameter ρ expressed as an expansion in the small wave number q: $\rho=\rho_1 q+\rho_2 q^2+\cdots$, and solving Eq. (21) at each order in the small wave number q, we find that $\rho_1=0=\rho_2=\rho_3$, and thus that the deviation ρ of the pumping parameter from its critical value must vary like q^4: $(1-k-u)(r-1)=(a/\sigma+1)^2\ q^4$. We deduce that above threshold a band of wave vectors q of width $(r-1)^{1/4}$ centered round $q_c=0$ is experiencing growth. The right scaling for the new spatial variables X and Y is then $X=(r-1)^{1/4}\,x$ and $Y=(r-1)^{1/4}\,y$. If we consider now a detuning slightly different from its critical value, namely, η small, then Eq. (21) is replaced at order one in ρ and two in q by the relation

$$(1-k-u)\rho+O(\rho^2)=\left[\frac{\eta-aq^2+(\sigma j+v)\rho}{\sigma+1}\right]^2[1+O(\rho)]. \tag{22}$$

η is considered as a small parameter and thus can be expressed as an expansion in the small wave number q: $\eta=\eta_1 q+\eta_2 q^2+\cdots$. In order to keep all of the relevant terms on the right-hand side of Eq. (22) and thus obtain a Swift-Hohenberg equation that takes into account all the physical parameters simultaneously, namely, the diffusion term $ia\nabla^2 e$ and the detuning η, we must consider that η is of order q^2. Therefore we impose $\eta_1=0$ and we deduce that η_2 must satisfy $(1-k-u)\rho_4=(\eta_2-a/\sigma+1)^2$. Since η varies like $(r-1)^{1/2}$, if the order of magnitude of η is called ϵ, we must choose $r=1+\epsilon^2$, and take $X=\sqrt{\epsilon}\,x$, and $Y=\sqrt{\epsilon}\,y$ for the spatial coordinates.

We need also to determinate the slow time scales. Following the same procedure as above, we can find the expressions of the real temporal growth rate s and of the frequency ω as expansions in the small wave number q. Starting from the dispersion relations Eq. (18) and Eq. (20) and looking for values of the parameters r, q, η, s, and ω close to their critical values, we obtain that the temporal growth rate and the frequency are linked to ρ and η through the relations

$$(\sigma+1)s_4=\sigma\left[(1-k-u)\rho_4-\left(\frac{\eta_2-a}{\sigma+1}\right)^2\right], \tag{23}$$

$$(\sigma+1)\omega_2=-[a+\sigma\eta_2]. \tag{24}$$

Since the frequency varies at the first order like $q^2=O(\epsilon)$ [Eq. (24)] and since the real temporal growth rate varies like $q^4=O(\epsilon^2)$ [Eq. (23)], the slow time scales necessary are $T_1=\epsilon\ t$ and $T_2=\epsilon^2\ t$.

B. Reduction to a Swift-Hohenberg equation

The slow time and space scales being determined, the calculations to derive a Swift-Hohenberg (SH) equation can be performed and are presented in Appendix C. It reads at order three in ϵ,

$$(\sigma+1)\frac{\partial\psi}{\partial t}=\sigma\left[(r-1)(1-k-u)\psi-\left(\frac{\eta+a\nabla^2}{\sigma+1}\right)^2\times\psi-(1+i\alpha)\frac{1}{b}|\psi^2|\psi\right]+i(a\nabla^2-\sigma\eta)\psi, \tag{25}$$

where the obtained alpha coefficient is defined as

$$\alpha=\frac{j-v}{1-k-u}. \tag{26}$$

To confirm that Eq. (25) models the same phenomena as Eq. (10), we have compared these two equations: identical threshold values and traveling wave solutions are found. Calculations are not presented here for the sake of brevity, but the procedure followed is analogous to the one used in Refs. [10] and [11]. Moreover, we have already mentioned that if we take all the parameters c,d,f,g,h,j,k,u,v equal to zero, the simplified MFEBE reduce exactly to the Maxwell-Bloch equations describing a two-level laser. When all of these parameters vanish, the detuning $\eta=\Omega+\sigma d$ becomes simply Ω and we recover exactly the Swift-Hohenberg equation for two-level lasers.

C. Characterization of the linewidth enhancement factor α

Using an intuitive derivation of the linewidth enhancement factor α [8], the following formula was obtained:

$$\alpha = -\frac{\dfrac{\partial \chi'}{\partial N}}{\dfrac{\partial \chi''}{\partial N}}. \tag{27}$$

As a consequence of the Lorentzian approximation of the susceptibility χ of the semiconductor medium [Eq. (1)], the linewidth enhancement factor deduced from Henry's formula Eq. (27) reads

$$\alpha = \frac{\chi_2' \Gamma_1 - \delta_2 \dfrac{A_1}{\Gamma_1}}{A_2 - \chi_2'' \Gamma_1 - \Gamma_2 \dfrac{A_1}{\Gamma_1}}.$$

However, using the definitions $j+ik=\chi_2\Gamma_1/A_2$ and $u+iv=(\Gamma_2+i\delta_2)\rho_1/A_2$, the deduced value of α from Eq. (26) is

$$\alpha = \frac{\chi_2' \Gamma_1 - \delta_2 \rho_1}{A_2 - \chi_2'' \Gamma_1 - \Gamma_2 \rho_1}.$$

Then the property $A_1/\Gamma_1=\rho_1$ valid for small values of the detuning (when $r_c \simeq 1$) leads to the same expression for the α factor as the expression deduced from Henry's formula. Therefore our method is consistent with Henry's approach of laser emission, and provides a way to calculate explicitly the coefficient α. Some values of the α factor for various lengths of laser and a mean reflectivity of the laser cavity $R=30\%$ are listed in Table I. These values are around $\alpha=-2$, which is consistent with experimental measurements.

TABLE I. Values of the coefficient α for various lengths of a laser.

L(μm)	α
100	-1.81
200	-1.98
250	-2.11
300	-2.25

D. Generalized equations in the stiff limit ($b \to 0$)

In the stiff limit of the Maxwell-Bloch equations, the derivation of a Swift-Hohenberg equation leads to two coupled order parameter equations [10,11]. This limit corresponds to a small decay rate of the population inversion and better describes a class B laser than the single SH equation derived by considering b finite. We have already mentioned that the simplified MFEBE have a form close to the form of the Maxwell-Bloch equations, and thus we can expect the simplified MFEBE to also give rise to coupled complex Swift-Hohenberg equations.

We need to repeat the procedure of Appendix C, taking into account the fact that b is small. The derivation of the coupled Swift-Hohenberg equations is given in Appendix D. They read at order four in ϵ,

$$(\sigma+1)\frac{\partial \psi}{\partial t} = \sigma\left\{[i(j+ik)+1-(u+iv)][(r-1)\psi - n\psi] - \left(\frac{\eta + a\nabla^2}{\sigma+1}\right)^2 \psi\right\} + i(a\nabla^2 - \sigma\eta)\psi,$$

$$\frac{\partial n}{\partial t} = c\nabla^2 n - bn + (1-f)|\psi|^2.$$

Here again we have compared the instability thresholds and the traveling wave solutions of the simplified MFEBE and of the coupled SH equations in order to check if both approaches describe the same physical problem. The same results are obtained, confirming that the reduction of the simplified MFEBE to the coupled SH equations is valid.

It is possible to obtain a system close to the coupled Swift-Hohenberg equations derived from the two-level Maxwell-Bloch equations, by introducing the change of order parameters

$$n \to \frac{n}{(1-k-u)},$$

$$\psi \to \frac{e^{i\sigma[(r-1)(1-k-u)/(1+\sigma)]}}{\sqrt{(1-k-u)(1-f)}}\psi.$$

Then the coupled Swift-Hohenberg equations take the form

$$(\sigma+1)\frac{\partial \psi}{\partial t} = \sigma\left[(r-1)(1-k-u)\psi - \left(\frac{\eta + a\nabla^2}{\sigma+1}\right)^2 \times \psi - (1+i\alpha)n\psi\right] + i(a\nabla^2 - \sigma\eta)\psi,$$

$$\frac{\partial n}{\partial t} = c\nabla^2 n - bn + |\psi|^2.$$

If we take the semiconductor coefficients c, $d+if$, $j+ik$, and $u+iv$ equal to zero we recover exactly the coupled Swift-Hohenberg equations in the case of a two-level laser. The model chosen in Ref. [12] corresponds to $c=0$ (no diffusion of the carrier density was considered) and $k+u=0$.

VI. CONCLUSION

In this paper we presented the derivation of a systematic approach for describing optical propagation in wide aperture edge and surface emitting semiconductor lasers. Inputs to the model include rigorously computed and experimentally validated gain and refractive index spectra parametrized by the total carrier density. The present analytic approach, based on a simple Lorentzian fit to the full semiconductor gain line shape, allows us to explicitly compute analytic coefficients for the various reduced laser models. The approach described here could also be applied to the raw computed gain and refractive index spectra or to experimental data, if available. The nonlinear partial differential equation model, its single

and longitudinal mode reductions include the important microscopic influences of peak gain shift and gain spectrum broadening with density variation. We have assumed that the temperature is fixed at room temperature in the present study. The latter restriction could be relaxed by providing gain and refractive index tables parametrized by carrier density and temperature and by adding a heat diffusion equation. In addition, we have obtained a reduced order-parameter equation description of a semiconductor laser that could be used to study wide-aperture VCSEL and VECSELs. The latter typically consist of multiple stacks of quantum wells and the increased gain per unit length can accommodate significantly greater facet losses than regular VCSELs.

Using changes of variables and a single mode approximation, we proved that the EBE generalized to counterpropagating waves can be reduced to the single-longitudinal mode MFEBE. The procedure also leads to a set of coupled mode equations that describe a multilongitudinal, multilateral mode broad area semiconductor laser. This description presents several advantages: in particular, in the single-longitudinal mode case, only three evolution equations instead of five are required. After having determined the lasing threshold through a linear stability analysis, linear expansions of the parameters involved in the nonlinear couplings were introduced, and a simplified form of the MFEBE was established.

We then presented the derivation of order parameter equations in the form of complex SH equations, suited to model the output of a wide-aperture single-longitudinal mode semiconductor laser such as a VCSEL. The slow time and space scales were determined through a linear stability analysis of the simplified MFEBE and from the characterization of the behavior of the neutral curves. Then the nonlinear analysis, using power series expansions in a small parameter ϵ linked to the distance between the pumping parameter r and its threshold value r_c, leads to the SH equation, or the coupled SH equations in the stiff limit. In this latter case, the model equations chosen in Ref. [12] in order to study the turbulence control in semiconductor lasers are placed on a sound footing. In particular, the empirical α factor introduced in Ref. [12] comes naturally in the derivation of the SH equation, and also agrees with Henry's definition [8] for the linewidth enhancement α factor.

ACKNOWLEDGMENTS

This work was supported by the U.S. Air Force under Contract No. F49620-00-1-0002 and, in part, by the National Science Foundation under Grant No. DMS 9811466.

APPENDIX A: EVOLUTION EQUATIONS FOR THE PERIODIC FIELD AMPLITUDES

In this appendix we will derive from the full counterpropagating field equations, governing equation for new variables adapted to Fourier decomposition. Taking the length of the cavity L as the reference length, the boundary conditions on the end mirrors are $E^+=\sqrt{R_1}\,E^-$ in $z=0$ and $E^-=\sqrt{R_2}\,E^+$ in $z=1$, where R_1 and R_2 are the reflectivity coefficients of the mirrors. Contrary to Ref. [19], no external injection is considered.

1. Change of variables

In the case of a unidirectional ring cavity, boundary conditions that involve both a time delay and a scaling of the field amplitude are obtained [18], preventing one from representing the cavity field as a linear superposition of orthogonal modal functions. In the case of a highly lossy semiconductor laser in a Fabry-Pérot geometry, the same problem is faced and boundary conditions involving a scaling of the counterpropagating electric fields are obtained [19]. In both cases, the problem is solved by introducing a suitable transformation of both the space-time coordinates and the dynamical variables, which allows an exact representation of the new variables as linear superpositions of orthogonal cavity functions in the transformed frame.

We consider the transformation of the dynamical variables,

$$E'^{+}=\frac{1}{\nu}e^{(1/2)z\ln R}E^+,$$

$$E'^{-}=\nu e^{-(1/2)z\ln R}E^-,$$

$$P'^{+}=\frac{1}{\nu}e^{(1/2)z\ln R}P^+,$$

$$P'^{-}=\nu e^{-(1/2)z\ln R}P^-,$$

where we have introduced the mean reflectivity of the Fabry-Pérot cavity $R=\sqrt{R_1R_2}$ and the normalization coefficient $\nu=R_1^{(1/4)}$. It may appear surprising that ν does not depend on R_2 since both mirrors should have symmetric influences. The symmetry can be easily recovered by changing z in $z-(1/2)$ in the transformation defined just above [then $\nu=(R_1/R_2)^{1/8}$]. The transformation chosen allows us to lighten the writings. Thanks to this transformation the boundary conditions become symmetric in the new frame, and the new field amplitudes obey standard ideal mirror boundary conditions $E'^{+}=E'^{-}$ in $z=0$ and $E'^{-}=E'^{+}$ in $z=1$. The transformed equations of motion

$$\frac{\partial E^\pm}{\partial t}=\frac{c}{n_gL}\left[\mp\frac{\partial E^\pm}{\partial z}-\frac{|\ln R|}{2}E^\pm\right]+\frac{ic}{2n_g}\left\{\frac{1}{K}\nabla^2E^\pm+K\Gamma\left[\chi_0(N)E^\pm+\frac{P^\pm}{\epsilon_0\epsilon_b}\right]\right\},\tag{A1}$$

$$\frac{\partial P^\pm}{\partial t}=\{-\Gamma_0(N)+i[\delta_0-\delta(N)]\}P^\pm-i\epsilon_0\epsilon_bA(N)E^\pm,\tag{A2}$$

$$\frac{\partial N}{\partial t}=D_N\nabla^2 N-\gamma_n N+\frac{\eta J}{ew}+\frac{i}{4\hbar}\left\{\epsilon_0\epsilon_b(\chi_0^*-\chi_0)\left[\nu^2|E^+|^2\times e^{-z\ln R}+\frac{1}{\nu^2}|E^-|^2e^{z\ln R}\right]+\nu^2(P^{+*}E^+-P^+E^{+*})\times e^{-z\ln R}+\frac{1}{\nu^2}(P^{-*}E^--P^-E^{-*})e^{z\ln R}\right\}, \tag{A3}$$

written with suppressing the primes contain both an additional electric field damping term $-c|\ln R|/2n_gLE^{\pm}$ as soon as both mirror are not perfect $(R\neq 1)$ contrary to the original set, and also an explicit spatial dependence through the exponential factors $e^{-z\ln R}$ and $e^{z\ln R}$.

2. Introduction of periodic variables

The electric field does not obey periodic boundary conditions, and a decomposition of Fourier type cannot be introduced. To solve this problem, we introduce a new electric field $\tilde{E}(x,y,z,t)$ which will be periodic. It is defined on a domain of twice the width of the Fabry-Pérot cavity and is equal to the forward electric field for positive values of the longitudinal coordinate $\tilde{E}(x,y,z,t)=E^+(x,y,z,t)$ if $z\in[0,1]$ and equal to the symmetric of the backward electric field with respect to the plane $z=0$ for negative values of z: $\tilde{E}(x,y,z,t)=E^-(x,y,-z,t)$ if $z\in[-1,0]$. This new electric field is a two-periodic function. The same transformation is applied to deduce the new polarization field $\tilde{P}$ from the initial polarization fields $P^{\pm}$. Because the carrier density is a scalar instead of a vector, the link between the new carrier density $\tilde{N}$ and N is different from the previous definitions. It is simply defined as $\tilde{N}(x,y,z,t)=N(x,y,z,t)$ if $z\in[0,1]$ and $\tilde{N}(x,y,z,t)=N(x,y,-z,t)$ if $z\in[-1,0]$. The next step consists in finding the evolution equations of $\tilde{E}$, $\tilde{P}$, and $\tilde{N}$.

3. Equations for the new periodic fields

The behaviors of the electric and polarization fields for $z\in[-1,0]$ are obtained by substituting z with $-z$ in Eqs. (A1) and (A2), and read

$$\frac{\partial\tilde{E}}{\partial t}+\frac{c}{n_gL}\frac{\partial\tilde{E}}{\partial z}=-\kappa\tilde{E}+\frac{ic}{2n_g}\left\{\frac{1}{K}\nabla^2\tilde{E}+K\Gamma\left[\chi_0(\tilde{N})\tilde{E}+\frac{\tilde{P}}{\epsilon_0\epsilon_b}\right]\right\},$$

$$\frac{\partial\tilde{P}}{\partial t}=\{-\Gamma_0(\tilde{N})+i[\delta_0-\delta(\tilde{N})]\}\tilde{P}-i\epsilon_0\epsilon_bA(\tilde{N})\tilde{E},$$

for $z\in[-1,1]$ where we have introduced the electric field damping coefficient

$$\kappa=\frac{c|\ln R|}{2n_gL}. \tag{A4}$$

For the carrier density, complications appear because of the explicit z dependance in Eq. (A3) through the exponential factors. Thus no evolution equations for the carrier density valid on the whole range $z\in[-1,1]$ can be derived. In the following, in order to simplify the notation the z dependence of the variables $\tilde{E}$, $\tilde{P}$, and $\tilde{N}$ will just be mentioned. We introduce the function f defined as

$$f(z)=\{\epsilon_0\epsilon_b[\chi_0^*(\tilde{N}(z))-\chi_0(\tilde{N}(z))]|\tilde{E}(z)|^2+\tilde{P}^*(z)\tilde{E}(z)-\tilde{P}(z)\tilde{E}^*(z)\}e^{-z\ln R},$$

and thus the evolution equation for the carrier density takes the simpler form

$$\frac{\partial\tilde{N}}{\partial t}=D_N\nabla^2\tilde{N}-\gamma_n\tilde{N}+\frac{\eta J}{ew}+\frac{i}{4\hbar}\left[\nu^2f(z)+\frac{1}{\nu^2}f(-z)\right], \tag{A5}$$

for $z\in[0,1]$. Substituting z with $-z$ in the previous equation leads to the evolution equation for the carrier density for $z\in[-1,0]$,

$$\frac{\partial\tilde{N}}{\partial t}=D_N\nabla^2\tilde{N}-\gamma_n\tilde{N}+\frac{\eta J}{ew}+\frac{i}{4\hbar}\left[\nu^2f(-z)+\frac{1}{\nu^2}f(z)\right]. \tag{A6}$$

These equations on the unfolded periodic domain can be very efficiently solved numerically using spectral methods.

APPENDIX B: MODAL DECOMPOSITION

1. General links between Fourier components

Fourier decomposition with respect to the z coordinate are introduced,

$$\begin{pmatrix}\tilde{E}(x,y,z,t)\\ \tilde{P}(x,y,z,t)\\ \tilde{N}(x,y,z,t)\end{pmatrix}=\sum_{j=-\infty}^{\infty}e^{i(k_jz-\omega_jt)}\begin{pmatrix}\tilde{E}_j(x,y,t)\\ \tilde{P}_j(x,y,t)\\ \tilde{N}_j(x,y,t)\end{pmatrix},$$

where the dimensionless wave numbers are selected such that $k_n=n\pi$, $n=0,\pm1,\pm2,\ldots$ in order to satisfy the periodic boundary conditions. The dimensional frequency of the nth mode is given by the dispersion relation $\omega_n=k_nc/n_gL$.

In order to keep on performing analytical calculations, explicit expressions of the nonlinear couplings between the electric field, the polarization field, and the carrier density are introduced. The nonlinear couplings appear through the carrier density dependence of the parameters involved in the Lorentzian approximation of the susceptibility. We will study the case of a linear dependence with respect to the carrier density of all these parameters,

$$\chi_0(N)=\chi_1+\chi_2N,$$

$$A(N)=A_1+A_2N,$$

$$\Gamma_0(N)=\Gamma_1+\Gamma_2 N,$$

$$\delta(N)=\delta_1+\delta_2 N.$$

Using the orthogonality property $\int_{-1}^{1} e^{i(k_j-k_n)z}dz=2\,\delta_{j,n}$, where $\delta_{j,n}$ designs the Krönecker delta, we obtain that the nth Fourier component $\tilde{E}_n$ obeys the following evolution equation:

$$\frac{\partial \tilde{E}_n}{\partial t}=-\kappa\tilde{E}_n+\frac{ic}{2n_g}\left\{\frac{1}{K}\nabla^2\tilde{E}_n + K\Gamma\left[\chi_1\tilde{E}_n+\chi_2\sum_i \tilde{N}_i\tilde{E}_{n-i}+\frac{\tilde{P}_n}{\epsilon_0\epsilon_b}\right]\right\},$$

and that $\tilde{P}_n$ obey the equation

$$\frac{\partial \tilde{P}_n}{\partial t}=[-\Gamma_1+i(\delta_0-\delta_1)]\tilde{P}_n-(\Gamma_2+i\delta_2)\times\sum_i \tilde{N}_i\tilde{P}_{n-i}-i\epsilon_0\epsilon_b\left[A_1\tilde{E}_n+A_2\sum_i \tilde{N}_i\tilde{E}_{n-i}\right].$$

The form of the carrier density $\tilde{N}$ evolution equation depends on the sign of the longitudinal coordinate z, which will complicate the obtention of the evolution equation of the nth Fourier components of the carrier density. By integrating Eq. (A5) between $z=0$ and $z=1$ and Eq. (A6) between $z=-1$ and $z=0$, by grouping together the terms containing $f(z)$, and the terms containing $f(-z)$, and finally by introducing the functions

$$I_n(\nu,R)=\int_0^1 f(z)e^{-i(k_nz-\omega_nt)}dz+\frac{1}{\nu^4}\times\int_{-1}^{0} f(z)e^{-i(k_nz-\omega_nt)}dz,$$

$$J_n(\nu,R)=\int_0^1 f(-z)e^{-i(k_nz-\omega_nt)}dz+\nu^4\times\int_{-1}^{0} f(-z)e^{-i(k_nz-\omega_nt)}dz,$$

we obtain for all integer n,

$$2\left(\frac{\partial \tilde{N}_n}{\partial t}-i\omega_n\tilde{N}_n\right)=\int_{-1}^{1}\left(D_N\nabla^2\tilde{N}-\gamma_n\tilde{N}+\frac{\eta J}{ew}\right)e^{-i(k_nz-\omega_nt)}dz+\frac{i}{4\hbar}\left[\nu^2 I_n(\nu,R)+\frac{J_n(\nu,R)}{\nu^2}\right].$$

The functions $(1/\sqrt{2})e^{ik_nz}$ where $k_n=n\pi$ with n are orthonormal only if the scalar product consists in an integration on the whole interval $z\in[-1,1]$. Therefore to use the orthogonality property, we need to make appear integrations on the range $z\in[-1,1]$ in the expressions of the functions $I_n(\nu,R)$ and $J_n(\nu,R)$, for example by writing

$$I_n(\nu,R)=\int_{-1}^{1} f(z)e^{-i(k_nz-\omega_nt)}\,dz+\left(\frac{1}{\nu^4}-1\right)K_n(R),$$

$$J_n(\nu,R)=\int_{-1}^{1} f(-z)e^{-i(k_nz-\omega_nt)}\,dz+(\nu^4-1)L_n(R),$$

where we have introduced the functions

$$K_n(R)=\int_{-1}^{0} f(z)e^{-i(k_nz-\omega_nt)}dz,$$

$$L_n(R)=\int_{-1}^{0} f(-z)e^{-i(k_nz-\omega_nt)}dz.$$

Like in the study of a ring cavity [18], we are led to introduce the mode-mode coupling coefficients in order to calculate all the scalar products involved between the function f and the exponential factors $e^{-i(k_nz-\omega_nt)}$,

$$\Gamma_p=\int_{-1}^{1} e^{ik_pz}e^{-z\ln R}dz=\frac{e^{ik_p}}{R}\frac{1-R^2}{ik_p-\ln R},$$

$$\Omega_p=\int_{-1}^{1} e^{ik_pz}e^{z\ln R}dz=\frac{e^{ik_p}}{R}\frac{1-R^2}{(-ik_p-\ln R)}.$$

Two mode-mode coupling coefficients have to be defined because we have to take into account forward and backward electric and polarization fields.

Using once again the Fourier expansions for the variables $\tilde{E}$, $\tilde{P}$, and $\tilde{N}$ and the orthogonality property we obtain that the nth Fourier component $\tilde{N}_n$ obeys

$$2\left(\frac{\partial \tilde{N}_n}{\partial t}-i\omega_n\tilde{N}_n\right)=2\left(D_N\nabla^2\tilde{N}_n-\gamma_n\tilde{N}_n+\frac{\eta J}{ew}\delta_{0,n}\right)+\frac{i}{4\hbar}\left[\nu^2 I_n(\nu,R)+\frac{1}{\nu^2}J_n(\nu,R)\right],\tag{B1}$$

where

$$I_n(\nu,R)=-2i\epsilon_0\epsilon_b\left(\chi_1''\sum_{i,j}\tilde{E}_i\tilde{E}_j^*\Gamma_{i-j-n}e^{-i\omega_{i-j-n}t}+\chi_2''\sum_{i,j,k}\tilde{N}_i\tilde{E}_j\tilde{E}_k^*\Gamma_{i+j-k-n}e^{-i\omega_{i+j-k-n}t}\right)+\sum_{i,j}\left(\tilde{P}_i^*\tilde{E}_j\Gamma_{-i+j-n}e^{-i\omega_{-i+j-n}t}-\tilde{P}_i\tilde{E}_j^*\Gamma_{i-j-n}e^{-i\omega_{i-j-n}t}\right)+\left(\frac{1}{\nu^4}-1\right)K_n(R),$$

$$J_n(\nu,R)=-2i\epsilon_0\epsilon_b\Bigg(\chi_1''\sum_{i,j}\tilde{E}_i\tilde{E}_j^*\Omega_{-i+j-n}e^{-i\omega_{i-j-n}t}+\chi_2''\sum_{i,j,k}\tilde{N}_i\tilde{E}_j\tilde{E}_k^*\Omega_{i-j+k-n}e^{-i\omega_{i+j-k-n}t}\Bigg)+\sum_{i,j}(\tilde{P}_i^*\tilde{E}_j\Omega_{i-j-n}e^{-i\omega_{-i+j-n}t}-\tilde{P}_i\tilde{E}_j^*\Omega_{-i+j-n}e^{-i\omega_{i-j-n}t})+(\nu^4-1)L_n(R).$$

The general case leads to take into account numerous interactions between the electric field, the polarization field, and the carrier density. However, in the limit case of perfect reflecting walls $R\to 1$, the mode-mode coupling coefficients reduce to delta coefficients $\Gamma_p=\lambda\,\delta_{0,p}$ and $\Omega_p=\lambda\,\delta_{0,p}$, where $\lambda=(1-R^2)/R|\ln R|$, and the normalization coefficient $\nu=R_1^{1/4}$ tends toward 1. As soon as $R\neq 0$ in order to have finite coefficients $e^{\pm z\ln R}$ (in particular, in the case of perfect reflecting walls $R\to 1$), the function f is bounded on $z\in[-1,1]$. Therefore both the products $(1/\nu^4-1)K_n(R)$ and $(\nu^4-1)L_n(R)$ are vanishing when the two end mirrors of the Fabry-Pérot cavity are taken perfectly reflecting. Then Eq. (B1) simplifies in the form

$$2\left(\frac{\partial\tilde{N}_n}{\partial t}-i\omega_n\tilde{N}_n\right)=2\left(D_N\nabla^2\tilde{N}_n-\gamma_n\tilde{N}_n+\frac{\eta J}{ew}\delta_{0,n}\right)+\frac{i\lambda}{4\hbar}\Bigg[-2i\epsilon_0\epsilon_b\Bigg(\chi_1''\sum_i\tilde{E}_i\tilde{E}_{i-n}^*+\chi_2''\sum_{i,j}\tilde{N}_i\tilde{E}_j\tilde{E}_{i+j-n}^*\Bigg)+\sum_i(\tilde{P}_i^*\tilde{E}_{i+n}-\tilde{P}_i\tilde{E}_{i-n}^*)-2i\epsilon_0\epsilon_b\times\Bigg(\chi_1''\sum_i\tilde{E}_i\tilde{E}_{i+n}^*e^{-i\omega_{-2n}t}+\chi_2''\sum_{i,j}\tilde{N}_i\tilde{E}_j\tilde{E}_{-i+j+n}^*e^{-i\omega_{2i-2n}t}\Bigg)+\sum_i(\tilde{P}_i^*\tilde{E}_{i-n}-\tilde{P}_i\tilde{E}_{i+n}^*)e^{-i\omega_{-2n}t}\Bigg].$$

2. Main Fourier order

The evolution equations of the amplitudes labeled by an index different from zero involve nonlinear terms that always include at least one amplitude labeled by an index $n\neq 0$. Therefore the amplitudes labeled by an index $n\neq 0$ remain equal to zero for all time if they are equal to zero at the initial time $t=0$. This means that we just have to take into account the zeroth Fourier modes, which leads to

$$\frac{\partial\tilde{E}_0}{\partial t}=-\kappa\tilde{E}_0+\frac{ic}{2n_g}\left\{\frac{1}{K}\nabla^2\tilde{E}_0+K\Gamma\left[\chi_1\tilde{E}_0+\chi_2\tilde{N}_0\tilde{E}_0+\frac{\tilde{P}_0}{\epsilon_0\epsilon_b}\right]\right\},$$

$$\frac{\partial\tilde{P}_0}{\partial t}=[-\Gamma_1+i(\delta_0-\delta_1)]\tilde{P}_0-(\Gamma_2+i\delta_2)\tilde{N}_0\tilde{P}_0-i\epsilon_0\epsilon_b[A_1\tilde{E}_0+A_2\tilde{N}_0\tilde{E}_0],$$

$$\frac{\partial\tilde{N}_0}{\partial t}=D_N\nabla^2\tilde{N}_0-\gamma_n\tilde{N}_0+\frac{\eta J}{ew}+\frac{i\lambda}{4\hbar}\{-2i\epsilon_0\epsilon_b[\chi_1''|E_0|^2+\chi_2''\tilde{N}_0|E_0|^2]+\tilde{P}_0^*\tilde{E}_0-\tilde{P}_0\tilde{E}_0^*\}.$$

Using the definition of the nth Fourier component, and introducing the usual mean-field quantities defined as $\langle E^\pm\rangle=\int_0^1E^\pm dz$, $\langle P^\pm\rangle=\int_0^1P^\pm dz$ and $\langle N\rangle=\int_0^1Ndz$, we obtain that the zeroth Fourier components are linked to the mean-field quantities by $E_0=(\langle E^+\rangle+\langle E^-\rangle)/2$, $P_0=(\langle P^+\rangle+\langle P^-\rangle)/2$ and $N_0=\langle N\rangle$. Suppressing the zero index, we have proved that the effective Bloch equations reduce to the mean-field model equations

$$\frac{\partial E}{\partial t}=-\kappa E+\frac{ic}{2n_g}\left\{\frac{1}{K}\nabla^2E+K\Gamma\left[\chi_0(N)E+\frac{P}{\epsilon_0\epsilon_b}\right]\right\},$$

$$\frac{\partial P}{\partial t}=\{-\Gamma_0(N)+i[\delta_0-\delta(N)]\}P-i\epsilon_0\epsilon_bA(N)E,$$

$$\frac{\partial N}{\partial t}=D_N\nabla^2N-\gamma_n(N-N_0)+\frac{i\lambda}{4\hbar}\{\epsilon_0\epsilon_b[\chi_0(N)^*-\chi_0(N)]|E|^2+P^*E-PE^*\}.$$

Instead of keeping the external injected current J, we have introduced the injected carrier density N_0 which is the particular value of the carrier density linked to the current J through the relation $(\eta J/ew)=\gamma_nN_0$. Although the mean field effective Bloch equations derived above are rigorously valid for $R\to 1$, they also remain valid for lossy semiconductor lasers.

APPENDIX C: DERIVATION OF THE SEMICONDUCTOR LASER SWIFT-HOHENBERG EQUATION

In this appendix we outline the derivation of the SH equation. Beyond threshold $r<1$ no laser emission exists and the solution of the simplified MFEBE is $(e,p,n)=(0,0,0)$. Slightly about threshold, at a small distance $\epsilon^2=r-1$, we can thus expect the solution (e,p,n) to be small. We assume that this solution is of order ϵ and look for solution in the form $(e,p,n)=\epsilon\,(e_1,p_1,n_1)+\epsilon^2(e_2,p_2,n_2)+\cdots$, where the (e_i,p_i,n_i)'s depend slowly on time and space.

We now plug these expressions into the simplified mean field effective Bloch equations, and identify the coefficients of powers of ϵ at each order. At order one, we get

$$\sigma e_1 = \sigma p_1,$$

$$p_1 = e_1,$$

$$b n_1 = 0,$$

which implies $n_1 = 0$. The solution is then $e_1 = p_1 = \psi$ where ψ is a complex variable. At order two, the simplified MFEBE yield

$$\left(\frac{\partial}{\partial T_1} - ia\nabla^2\right) e_1 = \sigma(p_2 - e_2),$$

$$\left(\frac{\partial}{\partial T_1} + i\eta_1\right) p_1 = e_2 - p_2,$$

$$b n_2 = \frac{1}{2}(e_1^* p_1 + e_1 p_1^*) - f\ |e_1|^2.$$

In terms of ψ, these equations read

$$\sigma(e_2 - p_2) = -\left(\frac{\partial}{\partial T_1} - ia\nabla^2\right)\psi,$$

$$(p_2 - e_2) = -\left(\frac{\partial}{\partial T_1} + i\eta_1\right)\psi,$$

$$b n_2 = (1-f)|\psi|^2.$$

The solvability condition for the first two equations involves a condition on ψ, which will be the dynamic equation sought for. It reads at this order

$$(\sigma+1)\frac{\partial \psi}{\partial T_1} = i(a\nabla^2 - \sigma\eta_1)\psi.$$

One can then choose $e_2 = 0$ and

$$p_2 = -\left(\frac{\partial}{\partial T_1} + i\eta_1\right)\psi,$$

$$n_2 = \frac{1-f}{b}|\psi|^2.$$

At next order, we get

$$\frac{\partial e_1}{\partial T_2} = \sigma[p_3 - e_3 + i(j+ik)(1-n_2)e_1],$$

$$\left(\frac{\partial}{\partial T_1} + i\eta_1\right)p_2 + \frac{\partial p_1}{\partial T_2} = e_3 - p_3 + (1-n_2)[e_1 - (u+iv)p_1],$$

$$b n_3 + \left(\frac{\partial}{\partial T_1} - c\nabla^2\right) n_2 = \frac{1}{2}(e_1^* p_2 + e_1 p_2^*),$$

which reads

$$\sigma(e_3 - p_3) = -\frac{\partial \psi}{\partial T_2} + \sigma i(j+ik)\left(1 - \frac{1-f}{b}|\psi|^2\right)\psi,$$

$$(p_3 - e_3) = -\frac{\partial \psi}{\partial T_2} + \left(\frac{\partial}{\partial T_1} + i\eta_1\right)^2 \psi + \left(1 - \frac{1-f}{b}|\psi|^2\right)[1-(u+iv)]\psi,$$

$$b n_3 = -\frac{1-f}{b}\left(\frac{\partial}{\partial T_1} - c\nabla^2\right)|\psi|^2 + \frac{ia}{2(\sigma+1)}(\psi\nabla^2\psi^* - \psi^*\nabla^2\psi),$$

and requires another solvability condition, which will give the behavior of ψ at the time scale T_2. Using the relation

$$\left(\frac{\partial}{\partial T_1} + i\eta_1\right)\psi = \frac{i}{(\sigma+1)}(\eta_1 + a\nabla^2)\psi,$$

the solvability condition reads

$$(\sigma+1)\frac{\partial \psi}{\partial T_2} = \sigma\left[-\left(\frac{\eta_1 + a\nabla^2}{\sigma+1}\right)^2 \psi + [i(j+ik)+1-(u+iv)] \times \left(1 - \frac{1-f}{b}|\psi|^2\right)\psi\right].$$

Again we choose $e_3 = 0$, and get for p_3 and n_3,

$$p_3 = \frac{1}{\sigma+1}\left\{-\left(\frac{\eta_1 + a\nabla^2}{\sigma+1}\right)^2 \psi + [1 - \sigma i(j+ik) - (u+iv)] \times \left(1 - \frac{1-f}{b}|\psi|^2\right)\psi\right\},$$

$$n_3 = \frac{ia}{b(\sigma+1)}\left(\frac{1}{2} + \frac{1-f}{b}\right)(\psi\nabla^2\psi^* - \psi^*\nabla^2\psi) + \frac{1-f}{b}c\nabla^2|\psi|^2.$$

The final equation for ψ is obtained by collecting all the terms and reads

$$(\sigma+1)\frac{\partial \psi}{\partial t} = (\sigma+1)\left[\epsilon\frac{\partial \psi}{\partial T_1} + \epsilon^2\frac{\partial \psi}{\partial T_2}\right].$$

One can get rid of the small parameter ϵ by reintroducing the original variables $x = X/\sqrt{\epsilon}$, $y = Y/\sqrt{\epsilon}$, $\eta = \epsilon\,\eta_1$, $r - 1 = \epsilon^2$, and redefining $\epsilon\,\psi$ as ψ. This yields an equation for ψ of the Swift-Hohenberg type

$$(\sigma+1)\frac{\partial \psi}{\partial t} = \sigma\left\{[i(j+ik)+1-(u+iv)] \times \left[(r-1)\psi - \frac{1-f}{b}|\psi|^2\psi\right] - \left(\frac{\eta + a\nabla^2}{\sigma+1}\right)^2\psi\right\} + i(a\nabla^2 - \sigma\eta)\psi.$$

We can also obtain the link between the order parameter ψ involved in the Swift-Hohenberg equation and the electric field e, the polarization field p, and the carrier density n appearing in the simplified MFEBE. Collecting all the terms corresponding to different powers of ϵ leads to

$$e=\epsilon e_1+\epsilon^2 e_2+\epsilon^3 e_3=\psi,$$

$$\begin{aligned} p&=\epsilon p_1+\epsilon^2 p_2+\epsilon^3 p_3 \\ &=\psi-\frac{i}{\sigma+1}(\eta+a\nabla^2)\psi+\frac{1}{\sigma+1}\left\{-\left(\frac{\eta+a\nabla^2}{\sigma+1}\right)^2\psi\right. \\ &\left.+[1-\sigma i(j+ik)-(u+iv)]\left(r-1-\frac{1-f}{b}|\psi|^2\right)\psi\right\}, \end{aligned}$$

$$\begin{aligned} n&=\epsilon^2 n_2+\epsilon^3 n_3 \\ &=\frac{1-f}{b}|\psi|^2+\frac{ia}{b(\sigma+1)}\left(\frac{1}{2}+\frac{1-f}{b}\right) \\ &\times(\psi\nabla^2\psi^*-\psi^*\nabla^2\psi)+\frac{1-f}{b}c\nabla^2|\psi|^2. \end{aligned}$$

Last, introducing the new order parameter

$$\tilde{\psi}=e^{-i\sigma[(r-1)(1-k-u)/(\sigma+1)]\alpha t\sqrt{(1-k-u)(1-f)}}\ \psi,$$

where the α coefficient is defined as $\alpha=j-v/1-k-u$, we obtain the simplified Swift-Hohenberg equation

$$\begin{aligned} (\sigma+1)\frac{\partial\tilde{\psi}}{\partial t}&=\sigma\left[(r-1)(1-k-u)\tilde{\psi}-\left(\frac{\eta+a\nabla^2}{\sigma+1}\right)^2\tilde{\psi}\right. \\ &\left.-(1+i\alpha)\frac{1}{b}|\tilde{\psi}^2|\tilde{\psi}\right]+i(a\nabla^2-\sigma\eta)\tilde{\psi}. \end{aligned}$$

APPENDIX D: DERIVATION OF THE COUPLED SH EQUATIONS IN THE STIFF LIMIT

We will now give details of the derivation of the two coupled equations which describe the semiconductor laser behavior in the stiff-limit of the simplified MFEBE.

As in the derivation of the semiconductor laser Swift-Hohenberg equations, we assume that the deviation from the critical detuning η is small, namely, $\eta=\epsilon\,\eta_1$. In addition, we suppose that the parameter b is now of order ϵ^2 (see Refs. [10,11]), i.e., $b=\epsilon^2\,b_2$, and that r is still given by $r=1+\epsilon^2$. We then introduce the spatial scales $X=\sqrt{\epsilon}\,x$, $Y=\sqrt{\epsilon}\,y$, and the two time scales $T_1=\epsilon\,t$ and $T_2=\epsilon^2\,t$.

Contrary to the case b of order 1, the expansion as a power series of ϵ of the solution (e,p,n) will not start at the first order: indeed if we look for traveling wave solution of the simplified MFEBE, Eq. (10) sought in the form $(e,p)=(\bar{e},\bar{p})\,e^{i(qx+\omega t)}$, $n=\bar{n}$, we can deduce that for a small value of the detuning η and for a pumping parameter close from its threshold value $r_c=1$ a traveling wave exists, associated with the expressions

$$\bar{n}=r-1-\frac{1}{1-k-u}\left(\frac{\eta-aq^2}{\sigma+1}\right)^2, \tag{D1}$$

$$\bar{e}^2=\frac{b}{1-f}\bar{n}, \tag{D2}$$

$$\begin{aligned} \bar{p}=&\left\{1-\frac{i}{\sigma+1}(\eta-aq^2)+\left[k-\frac{i}{\sigma+1}(\sigma j+v)\right]\right. \\ &\left.\times\frac{1}{1-k-u}\left(\frac{\eta-aq^2}{\sigma+1}\right)^2\right\}\bar{e}. \end{aligned} \tag{D3}$$

The carrier density is of second order in ϵ [Eq. (D1)]. Since b is of order ϵ^2, Eq. (D2) leads to $\bar{e}$ of order ϵ^2. Equation (D3) indicates that at the lowest order in ϵ the value of the polarization fields $\bar{p}$ is of the same order as the value of the electric field $\bar{e}$. Therefore we look for expansions of e, p, and n as power series of ϵ started at the second order, namely,

$$(e,p,n)=\epsilon^2(e_2,p_2,n_2)+\epsilon^3\ (e_3,p_3,n_3)+\cdots.$$

At order two, we get

$$\sigma e_2=\sigma p_2,$$

$$p_2=e_2,$$

$$0=0,$$

which gives $e_2=p_2=\psi$ and the equations at order three are

$$\left(\frac{\partial}{\partial T_1}-ia\nabla^2\right)e_2=\sigma(p_3-e_3),$$

$$\left(\frac{\partial}{\partial T_1}+i\eta_1\right)p_2=e_3-p_3,$$

$$\left(\frac{\partial}{\partial T_1}-c\nabla^2\right)n_2=0,$$

which read in terms of the complex variable ψ,

$$\sigma(e_3-p_3)=-\left(\frac{\partial}{\partial T_1}-ia\nabla^2\right)\psi,$$

$$(p_3-e_3)=-\left(\frac{\partial}{\partial T_1}+i\eta_1\right)\psi,$$

$$\left(\frac{\partial}{\partial T_1}-c\nabla^2\right)n_2=0.$$

The compatibility of the first two equations requires the following solvability condition, which describes the variations of ψ at the time scale T_1:

$$(\sigma+1)\frac{\partial\psi}{\partial T_1}=i(a\nabla^2-\sigma\eta_1)\psi. \tag{D4}$$

We can then choose $e_3=0$ and

$$p_3 = -\left(\frac{\partial}{\partial T_1} + i\eta_1\right)\psi = -\frac{i}{(\sigma+1)}(\eta_1 + a\nabla^2)\psi.$$

At fourth order,

$$\frac{\partial e_2}{\partial T_2} = \sigma[p_4 - e_4 + i(j+ik)(1-n_2)e_2],$$

$$\left(\frac{\partial}{\partial T_1} + i\eta_1\right)p_3 + \frac{\partial p_2}{\partial T_2} = e_4 - p_4 + (1-n_2)[e_2 - (u+iv)p_2],$$

$$\left(\frac{\partial}{\partial T_2} + b_2\right)n_2 + \left(\frac{\partial}{\partial T_1} - c\nabla^2\right)n_3 = \frac{1}{2}(e_2^* p_2 + e_2 p_2^*) - f|e_2|^2,$$

i.e.,

$$\sigma(e_4 - p_4) = -\frac{\partial\psi}{\partial T_2} + \sigma i(j+ik)(1-n_2)\psi,$$

$$(p_4 - e_4) = -\frac{\partial\psi}{\partial T_2} + \left(\frac{\partial}{\partial T_1} + i\eta_1\right)^2 \times \psi + (1-n_2)[1-(u+iv)]\psi,$$

$$\left(\frac{\partial}{\partial T_1} - c\nabla^2\right)n_3 + \frac{\partial n_2}{\partial T_2} = -b_2 n_2 + (1-f)|\psi|^2.$$

Again we obtain the following solvability condition:

$$(\sigma+1)\frac{\partial\psi}{\partial T_2} = \sigma\left\{-\left(\frac{\eta_1 + a\nabla^2}{\sigma+1}\right)^2\psi + [i(j+ik)+1 - (u+iv)](1-n_2)\psi\right\}. \quad \text{(D5)}$$

We can choose $e_4 = 0$ and calculate

$$p_4 = \frac{1}{\sigma+1}\left\{-\left(\frac{\eta_1 + a\nabla^2}{\sigma+1}\right)^2\psi + [1 - \sigma i(j+ik) - (u+iv)](1-n_2)\psi\right\}.$$

We now can collect all the terms and get the equation for ψ,

$$(\sigma+1)\frac{\partial\psi}{\partial t} = (\sigma+1)\left[\epsilon\frac{\partial\psi}{\partial T_1} + \epsilon^2\frac{\partial\psi}{\partial T_2}\right].$$

The spatial derivatives in Eqs. (D4) and (D5) are derivatives with respect to the slow scales $X = \sqrt{\epsilon}x$ and $Y = \sqrt{\epsilon}y$. Any term of the form $\epsilon\nabla^2$ then corresponds to ∇^2 in terms of spatial derivatives with respect to x and y. Letting $n = \epsilon^2 n_2 + \epsilon^3 n_3$ we get

$$(\sigma+1)\frac{\partial\psi}{\partial t} = \sigma\left\{[i(j+ik)+1-(u+iv)][(r-1)\psi - n\psi] - \left(\frac{\eta + a\nabla^2}{\sigma+1}\right)^2\psi\right\} + i(a\nabla^2 - \sigma\eta)\psi.$$

Similarly, the equation for n is

$$\frac{\partial n}{\partial t} = \epsilon^3\frac{\partial n_2}{\partial T_1} + \epsilon^4\left(\frac{\partial n_3}{\partial T_1} + \frac{\partial n_2}{\partial T_2}\right) = c\nabla^2(\epsilon^2 n_2 + \epsilon^3 n_3) + \epsilon^4[-b_2 n_2 + (1-f)|\psi|^2],$$

i.e., in terms of the original variables and redefining $\epsilon^2\psi$ as ψ,

$$\frac{\partial n}{\partial t} = c\nabla^2 n - bn + (1-f)|\psi|^2.$$

Finally, the expressions of e and p versus ψ are

$$e = \epsilon e_1 + \epsilon^2 e_2 + \epsilon^3 e_3 = \psi,$$

$$p = \epsilon p_1 + \epsilon^2 p_2 + \epsilon^3 p_3 = \psi - \frac{i}{\sigma+1}(\eta + a\nabla^2)\psi + \frac{1}{\sigma+1} \times \left\{-\left(\frac{\eta + a\nabla^2}{\sigma+1}\right)^2\psi + [1 - \sigma i(j+ik) - (u+iv)](r-1-n)\psi\right\}.$$

[1] W.W. Chow, S.W. Koch, and M. Sargent, *Semiconductor Laser Physics* (Springer-Verlag, Berlin, 1994).

[2] H. Haug and S.W. Koch, *Quantum Theory of the Optical and Electronic Properties of Semiconductors*, 2nd ed. (World Scientific, Singapore, 1993).

[3] W.W. Chow and S.W. Koch, *Semiconductor Laser Fundamentals: Physics of the Gain Materials* (Springer-Verlag, Berlin, 1999).

[4] C. Ellmers, A. Girndt, M. Hoffmann, A. Knorr, W.W. Ruhle, F. Jahnke, S.W. Koch, C. Hanke, L. Korte, and C. Hoyer, Appl. Phys. Lett. **72**, 1647 (1998).

[5] W.W. Chow, P.M. Smowton, P. Blood, A. Girndt, F. Jahnke, and S.W. Koch, Appl. Phys. Lett. **71**, 157 (1997).

[6] J. Hader, D. Bossert, J. Stohs, W.W. Chow, S.W. Koch, and J.V. Moloney, Appl. Phys. Lett. **74**, 2277 (1999).

[7] J. Hader, S.W. Koch, J.V. Moloney, and E.P. O'Reilly, Appl. Phys. Lett. **77**, 630 (2000).

[8] C.H. Henry, IEEE J. Quantum Electron. **QE-18**, 259 (1982).

[9] T. Rossler, R.A. Indik, G.K. Harkness, J.V. Moloney, and C.Z. Ning, Phys. Rev. A **58**, 3279 (1998).

[10] J. Lega, J.V. Moloney, and A.C. Newell, Phys. Rev. Lett. **73**, 2978 (1994).

[11] J. Lega, J.V. Moloney, and A.C. Newell, Physica D **83**, 478 (1995).

[12] D. Hochheiser, J.V. Moloney, and J. Lega, Phys. Rev. A **55**, R4011 (1997).
[13] S. Balle, Phys. Rev. A **57**, 1304 (1998).
[14] L.A. Lugiato, C. Oldano, and L.M. Narducci, J. Opt. Soc. Am. B **5**, 879 (1988).
[15] C.Z. Ning, R.A. Indik, and J.V. Moloney, IEEE J. Quantum Electron. **33**, 1543 (1997).
[16] S. Hughes, A. Knorr, S.W. Koch, R. Binder, R.A. Indik, and J.V. Moloney, Solid State Commun. **100**, 555 (1996).
[17] J.V. Moloney, R.A. Indik, and C.Z. Ning, IEEE Photonics Technol. Lett. **9**, 731 (1997).
[18] L.A. Lugiato, L.M. Narducci, D.K. Bandy, and J.R. Tredicce, Phys. Rev. A **33**, 1109 (1986).
[19] P. Ru, J.V. Moloney, and R. Indik, Phys. Rev. A **50**, 831 (1994).
[20] P.K. Jakobsen, J.V. Moloney, A.C. Newell, and R. Indik, Phys. Rev. A **45**, 8129 (1992).
[21] L.A. Lugiato, C. Oldano, and L.M. Narducci, J. Opt. Soc. Am. B **5**, 879 (1988).
[22] A.C. Newell and J.V. Moloney, *Nonlinear Optics* (Addison-Wesley, Redwood City, CA, 1992).